XXXVI Ibero-Latin American Congress on Computational Methods in Engineering
CILAMCE
Rio de Janeiro, 22-25 Nov 2015

APPLICATION OF A 2D EQUIVALENT CONTINUUM APPROACH TO THE ASSESSMENT OF GEOLOGICAL FAULT REACTIVATION IN RESERVOIRS

Mejia Sanchez, Eleazar C.

Pezo Zegarra, Eliot

Oliveira, Maria F. F.

Roehl, Deane

crisms@tecgraf.puc-rio.br

peliotz@tecgraf.puc-rio.br

mariafer@tecgraf.puc-rio.br

droehl@puc-rio.br

Tecgraf Institute and Civil Engineering Department of PUC-Rio

Rua Marques de São Vicente, 225, Gávea, 22453900, Rio de Janeiro, RJ, Brasil.

Abstract. *The reactivation of geological faults in oil and gas reservoirs may have severe consequences as seismicity, well collapse and breach of seal integrity. During fluid production/injection, the stress state of the surrounding formation is modified, which may induce slippage and reactivation of preexisting faults. This paper presents the application of an equivalent continuum approach with the finite element method for the analysis of fault instability. The equivalent continuum formulation is based on the principle of deformation equivalence with Mohr-Coulomb criterion for rock and fault. Some synthetic models of a reservoir crossed by a fault were analyzed for several fault dip angles, for both injection and depletion cases. Results were compared with models that explicitly considered faults as interface elements. The studied methodology can be an attractive alternative to model fault reactivation in geomechanical problems.*

Keywords: *Geological fault reactivation, equivalent continuum model, geomechanical analysis, finite element model.*

1 INTRODUCTION

During the production process of an oil and gas field, fluid injection and depletion modify the stress state of the reservoir and its surrounding rock formation, including preexisting geological faults. If the stress components acting on a fault plane are sufficiently altered, the fault may slip and reactivate (Byerlee, 1978; Sibson, 1977).

The slippage of a geological fault may aggravate land subsidence, induce seismicity and cause well collapse, as reported in several field observations (Segall et al, 1994; Morton, R. A. et al, 2006; Chan & Zoback, 2007). In addition, the reactivation may breach the extensional seal of the fault by modifying its permeability, thus allowing fluid migration (Wiprut & Zoback, 2000; Faulkner, 2010). In this condition, even juxtaposed porous layers may communicate and eventually, fluid leakage may occur (Chen et al., 2013). To prevent from these severe damages, the assessment of fault reactivation is a necessary step in the definition of a reservoir production scheme.

Fault stability can be evaluated by testing the stress state on the fault plane against a reactivation criterion. This stress state can be obtained from either simple analytical predictions or geomechanical model simulations. However, if the relative movement of the discontinuity in the fault plane is not taken into account, slippage may be underestimated, especially in shear zones.

In the finite element modeling, this desired deformational behavior of the fault discontinuity can be modelled with interface elements, as suggested by Goodman et al. (1968). This approach has been adopted in Costa (1984) and Rueda et al. (2014). The pore-pressure-mechanical coupling can also be considered, as proposed by Ng & Small (1997). Nevertheless, discretization with interface elements requires the mesh to conform with the irregular geometry of the faults, which may be a cumbersome task, especially in three-dimensions. In some cases, several simplifications in the representation of the field geology are necessary to accomplish a regular quality mesh with acceptable computational cost.

This paper investigates the application of a continuum equivalent approach with the finite element method to evaluate geological fault stability. The formulation is based on the principle of deformation equivalence with the Mohr-Coulomb envelope as failure criteria. This approach leads to an anisotropic compliance matrix that takes into account both the isotropic rock behavior and the presence of the fault plane (Zhu & Zhao, 2004). The rock formation finite elements intercepted by a geological fault in the model will have modified deformational and strength parameters. Notice that this procedure requires only the identification of those finite elements that are intercepted by the fault and the determination of the geometry of the intercept — there is no need to explicitly discretize the fault in the mesh.

2 AN EQUIVALENT CONTINUUM FORMULATION FOR FAULTED ROCKS

The 2D equivalent continuum approach adopted in this study is based on the principle of equivalent displacements, which assumes that for a given stress state, the displacement of a continuum equivalent mass is equal to that of the intact rock mass with a fault discontinuity (Zhu & Zhao, 2004; Rueda et al., 2014, Pezo et al., 2013).

Following this approach, the total displacement of an equivalent continuum element can be written as

$$\delta_i = \delta_i^R + \delta_i^F \tag{1}$$

where δ_i^R is the displacement of the intact rock and δ_i^F is the relative displacement on the fault plane.

Figure 1 illustrates a continuum equivalent element (a) and the intact rock crossed by a fault (b). Assuming the intact rock as isotropic, its corresponding elastic compliance matrix is given according to Hooke's law as $\boldsymbol{\varepsilon}^{\mathbf{R}} = \mathbf{C}^{\mathbf{R}}.\,\boldsymbol{\sigma}$, where $\mathbf{C}^{\mathbf{R}}$ is the compliance elastic tensor.

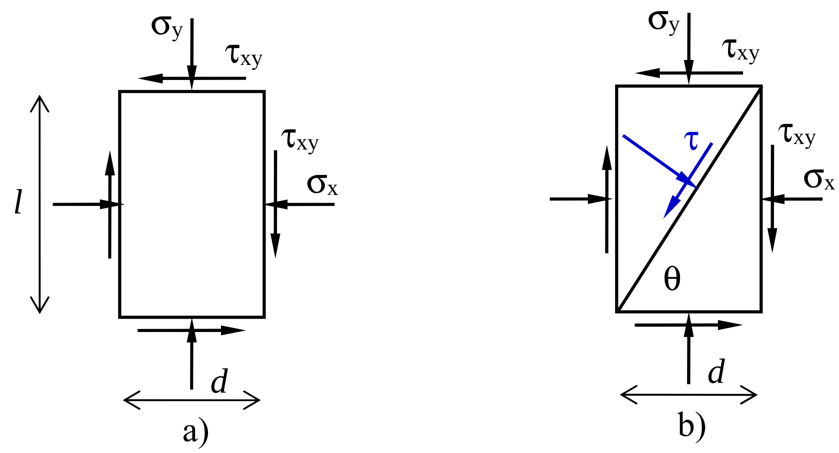

Figure 1. A 2D continuum equivalent element (a) and an intact rock mass crossed by a fault (b).

For a fault with dip angle θ as shown in Fig. 1b, the normal stress σ_n and shear stress τ on the fault plane are given as

$$\begin{Bmatrix} \sigma_n \\ \tau \end{Bmatrix} = \begin{Bmatrix} \sigma_x.\sin^2\theta + \sigma_y.\cos^2\theta - \tau_{xy}.\sin 2\theta \\ (\sigma_y - \sigma_x).\sin\theta.\cos\theta + \tau_{xy}.\cos 2\theta \end{Bmatrix} \tag{2}$$

Assuming an uncoupled traction-separation behavior for the fault, the relative displacements on the fault plane in global coordinates are determined as,

$$\begin{Bmatrix} \delta_x^F \\ \delta_y^F \end{Bmatrix} = \begin{Bmatrix} \dfrac{\sigma_n}{k_n}.\sin\theta - \dfrac{\tau}{k_s}.\cos\theta \\ \dfrac{\sigma_n}{k_n}.\cos\theta + \dfrac{\tau}{k_s}.\sin\theta \end{Bmatrix} \tag{3}$$

where k_n and k_s are the normal and shear stiffness parameters of the fault region, respectively.

Applying the principle of equivalent displacement leads to an equivalent continuum element that is anisotropic with a compliance matrix $\mathbf{C}^{\mathbf{eq}}$ expressed as

$$\left.\begin{aligned}
C_{11}^{eq} &= C_{11}^{R} + \frac{\sin\theta^3}{k_n.d} + \frac{\sin\theta.\cos\theta}{k_s.d} \\
C_{12}^{eq} &= C_{12}^{R} + \frac{\cos\theta^2.\sin\theta}{k_n.d} - \frac{\sin\theta.\cos\theta^2}{k_s.d} \\
C_{13}^{eq} &= C_{13}^{R} - \frac{\sin 2\theta.\cos\theta}{k_n.d} + \frac{\cos 2\theta.\cos\theta}{k_s.d} \\
C_{22}^{eq} &= C_{22}^{R} + \frac{\cos\theta^3}{k_n.l} + \frac{\sin\theta^2.\cos\theta}{k_s.l} \\
C_{23}^{eq} &= C_{23}^{R} - \frac{\sin\theta^3}{k_n.l} + \frac{\cos\theta^2.\sin\theta}{k_s.l}
\end{aligned}\right\} \tag{4}$$

where, $C_{12}^{eq} = C_{21}^{eq}$, $C_{13}^{eq} = C_{31}^{eq}$ and $C_{23}^{eq} = C_{32}^{eq}$ if $l = d\tan\theta$; $C_{33}^{eq} = 1/G$, being G the shear modulus of the intact rock. The strain increment vector is calculated using the equivalent compliance matrix as (Pezo et al., 2013),

$$\Delta\varepsilon = C^{eq}.\Delta\sigma \tag{5}$$

The strength of the continuum equivalent mass is governed by both the strength of the intact rock mass and the fault. According to the Mohr-Coulomb criterion, the failure of a rock will occur along the plane of maximum shear stress if the following condition is satisfied

$$\frac{\sigma_1 - \sigma_3}{2} - \frac{\sigma_1 - \sigma_3}{2}\sin\varphi_{eq} = c_{eq}.\cos\varphi_{eq} \tag{6}$$

where φ_{eq} and c_{eq} are the cohesion and the friction angle of the equivalent rock mass, respectively. Assuming a persistent fault within the rock element, the equivalent strength parameters can be chosen from the expression below in order to obtain the critical envelope.

$$\left.\begin{aligned}
\varphi_{eq} &= \sin^{-1}\frac{\sin(\varphi_f)}{\sin(2\beta - \varphi_f)} \\
c_{eq} &= c_f.\frac{\cos(\varphi_f)}{\sin(2\beta - \varphi_f).\cos(\varphi_{eq})}
\end{aligned}
\quad or \quad
\begin{aligned}
\varphi_{eq} &= \varphi_R \\
c_{eq} &= c_R
\end{aligned}\right\} \tag{7}$$

where (c_r, φ_r), (c_f, φ_f) are the Mohr-Coulomb parameters of the intact rock and of the fault, respectively.

According to Byerlee's law, the reactivation of a geological fault is ruled by the Mohr-Coulomb criterion. In the assessment of fault reactivation, it is useful to evaluate the slip tendency parameter 'ST' which is defined as the ratio between the acting shear stress τ_s and the slip shear stress τ_{slip} (Byerlee, 1978)

$$ST = \tau_s / \tau_{slip}, \quad 0 \le ST \le 1 \tag{8}$$

Faults are considered to reactivate when ST reaches the upper limit, i.e. ST=1.

The elastoplastic constitutive model for the equivalent continuum element described above was implemented in a specific UMAT subroutine for the program Abaqus®.

3 GEOMECHANICAL FINITE ELEMENT MODELS

Figure 2 a and b show the analyzed synthetic cross-sections, with an embedded reservoir intercepted by a single fault at 37° and 60°, respectively.

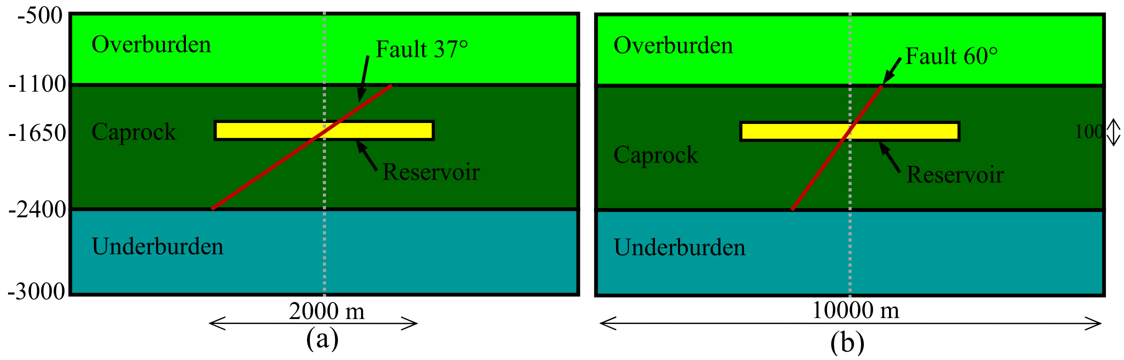

Figure 2. Synthetic models a) with a fault at 37 ° and b) with a fault at 60°.

Table 1 presents the deformational and strength rock properties, in which *E* is Young's modulus, ν is Poisson's ratio, c_r the cohesion, φ_r the friction angle, and α Biot's coefficient.

Table 2 presents the cohesion c_f, the friction angle φ_f, the tangential and normal stiffness values (k_t and k_n) for each fault extension crossing the rock layers. Fault extensions were considered sealed except for the regions within the reservoir, for which Biot's coefficient is α = 1.0.

Table 1. Rock properties.

Layer	E GPa	ν	c_r MPa	φ_r (°)	α
Overburden	5.00	0.260	5.15	30.00	----
Caprock	3.60	0.36	5.15	28.36	----
Reservoir	5.29	0.36	4.69	28.82	1.00
Underburden	25.00	0.36	5.15	30.00	----

Table 2. Fault properties.

Layer	k_n GPa/m	k_t GPa/m	c_f MPa	φ_f (°)
Caprock	3.6	1.32	0.5	18.36
Reservoir	5.29	1.95	0.5	10

The in situ stresses were initialized with a constant vertical effective stress gradient of 10.0 kN/m^2/m and a lateral coefficient of 0.7 for the horizontal effective stresses. Two pre-defined pore pressure scenarios were considered: injection and depletion, both with a constant pore-pressure distribution in the reservoir.

For the sake of comparison, these models were analyzed in two different ways: by implicitly representing the fault with equivalent continuum elements and by explicitly representing the fault with interface elements. Figure 3 shows a finite element mesh and the vertical in situ stress field of the section with the 37-degrees dip angle fault for each approach.

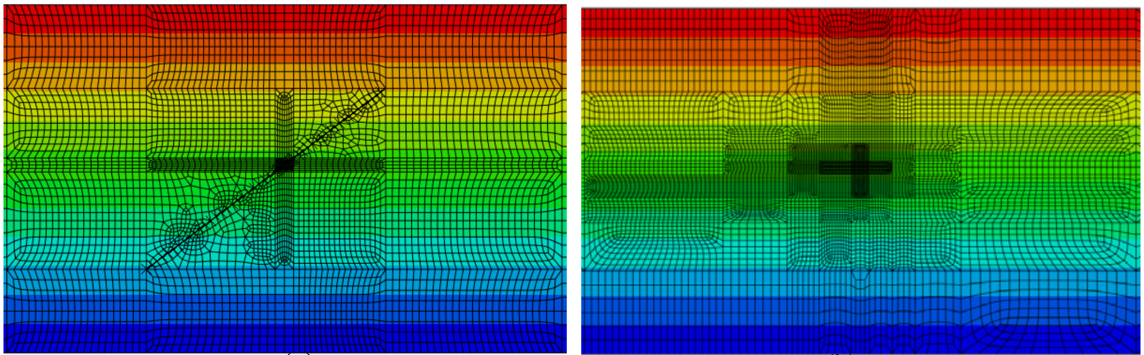

(a) (b)

Figure 3. The in situ vertical stress field for models with faults represented explicitly (a) and implicitly (b).

The mesh is refined in order to analyze its influence on the results. A fine and a coarse mesh were considered for the equivalent continuum approach, as shown in Fig. 4. On the other hand, for the interface element approach, a fine mesh was considered as a reference model (Chen, 2012).

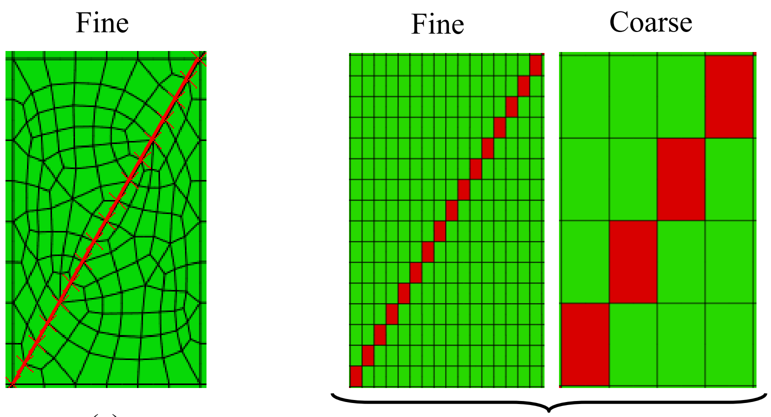

(a) (b)

Figure 4. Mesh refinement for: a) the interface element approach b) the CE approach.

The geomechanical FE simulations were carried out in effective stresses using the FE commercial software ABAQUS®, with implemented user subroutines of type UEL for the interface element (Rueda, 2013) and of type UMAT for the equivalent continuum element.

4 NUMERICAL RESULTS

The numerical results for fault reactivation using Abaqus® for the interface element and the CE element approaches are compared as shown below. Figure 5 - 8 shows the slip tendency at the first gauss point to reach the ST=1, so called as the reactivation point, for the injection and depletion cases, for both synthetic cross-sections.

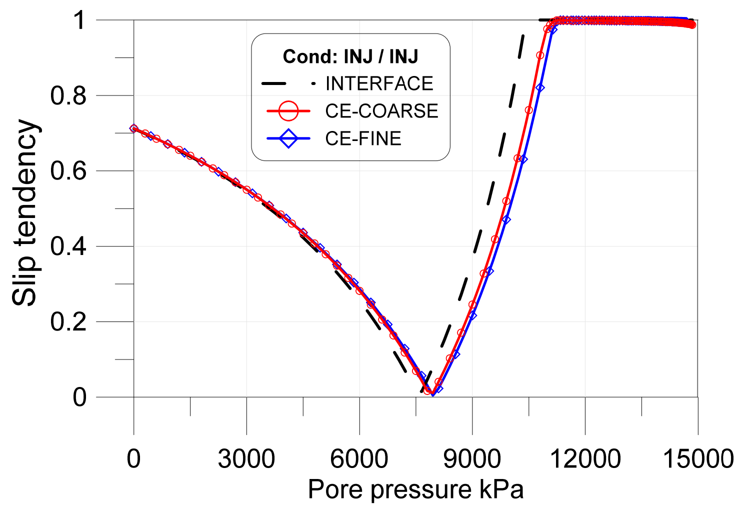

Figure 5. Slip tendency for the 37-degrees fault under injection.

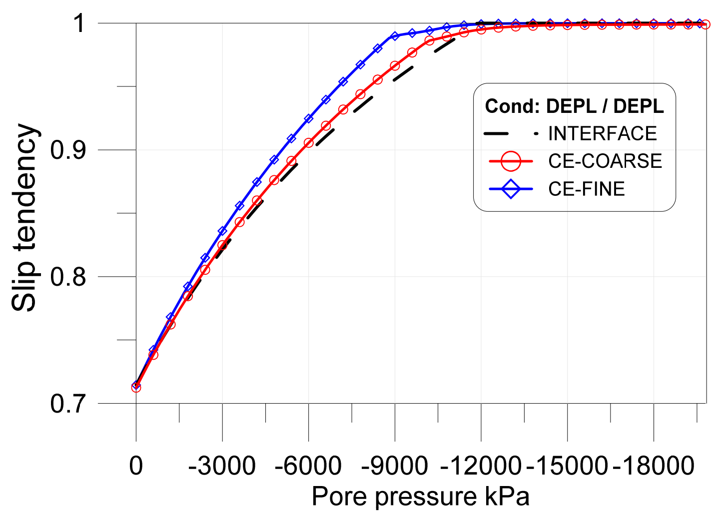

Figure 6. Slip tendency for the 37 degrees fault under depletion.

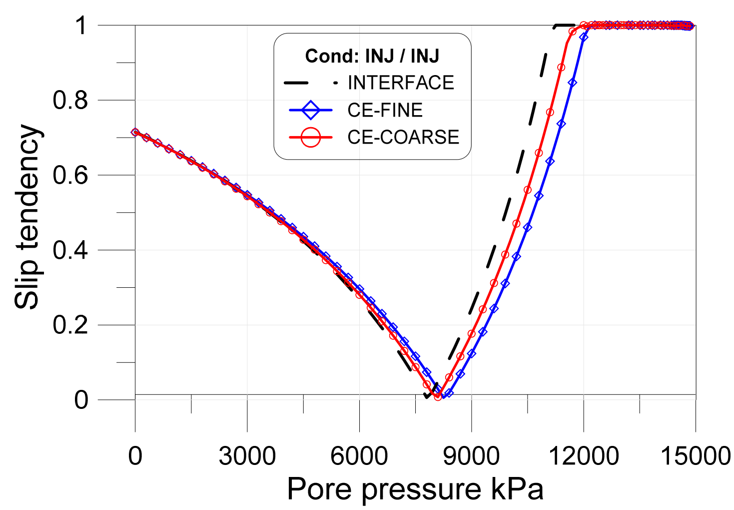

Figure 7. Slip tendency for the 60 degrees fault under injection.

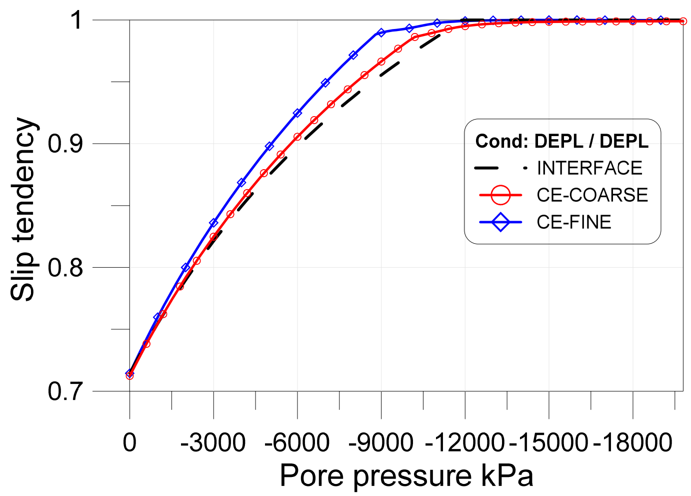

Figure 8. Slip tendency for the 60 degrees fault under depletion.

The table 3 summarizes the results of fault reactivation for both values of the fault dip angle in the injection scenario.

Table 3. Comparison of numerical results in the injection scenario.

Fault angle	Δp of fault reactivation (kPa)		
	CE - Coarse	CE - Fine	Interface
37°	11064	11193	10500
60°	11700	12150	11250

5 CONCLUDING REMARKS

In this work, the numerical results obtained with a refined mesh of interface elements are used as a reference to validate the equivalent continuum approach. The failure criterion based on the Mohr-Coulomb envelop with equivalent smeared parameters was successful in determining critical pressure changes in the reservoir that would lead to fault reactivation.

Results obtained by using the equivalent continuum element and the interface element for some synthetic models were compared and showed good approximation. According to the slip tendency ratio shown in Fig. 7 and the pore pressure for fault reactivation in Tab. 3, the equivalent continuum element presented better results with the coarse mesh than with the fine mesh. This approach presents the well known problem of non-objectivity of the mesh, typical of models with material softening behavior. Further studies to evaluate adequate meshes are in progress.

Finally, this study demonstrates that the equivalent continuum element can serve as an attractive alternative to model fault reactivation in geomechanical problems.

ACKNOWLEDGEMENTS

This research has been generously supported by Petrobras S.A. This support is gratefully acknowledged.

REFERENCES

Byerlee, J., 1978. Friction of rocks. *Pageoph*, vol. 116, pp. 615–626.

Chan, A. W., & Zoback, M. D., 2007. The role of hydrocarbon production on land subsidence and fault reactivation in the Loiusiana Coastal Zone. *Journal of Coastal Research*, v. 24, pp. 771–786.

Chen, M., Buscheck, T. A., Wagoner, J. L., Sun, Y., White, J. A., Chiaramonte, L., & Aines, R. D., 2012. Analysis of fault leakage from Leroy underground natural gas storage facility, Wyoming, USA. *Hydrogeology Journal,* vol. 21, pp. 1429–1445.

Chen, Z., 2012. Finite element modelling of viscosity-dominated hydraulic fractures., USA. *Journal of Petroleum Science and Engineering,* vol. 88-89, pp. 136–144.

Costa, A. M., 1984. An application of computational methods and principles of rock mechanics in the design and analysis of underground excavations for the underground mining, *Phd Thesis, Graduate school of Engineering* COPPE), Federal University of Rio de Janeiro (UFRJ).

Faulkner, D. R; Jackson, C. A. L.; Lunn, R. J.; Schlische, R. W.; Shipton, Z. K.; Wibberley, C. A. J.; & Withjack, M. O., 2010. A review on recent developments concerning the structure, mechanics and fluid flow properties of fault zones. *Journal of Structural Geology*, vol. 32, 1557–1575.

Goodman, E. L.; Taylor, R. L.; & Brekke, A. M., 1968. A model for the mechanics of jointed rock. *Journal of Soil and Mechanics and Foundation Engineering*, vol. 94, 637–659.

Morton, R. A., Bernier, J. C., & Barras, J. A, 2006. Evidence of regional subsidence and associated interior wetland loss induced by hydrocarbon production, Gulf Coast region, USA. *Environmental Geology*, vol. 50, 261–274.

Ng, K. L. A.; & Small, J. C., 1997. Behavior of Joints and Interfaces Subjected to Water Pressure. *Computers and Geotechnics*, vol. 20, pp. 71–93.

Pezo, E., Noreña, N., Roehl, D. M., & Romanel, C., 2013. Modelo do continuo equivalente para junta em maciço de rocha fracturado. In: *XXXIV Iberian Latin American Congress on Computational Methods in Engineering* (*CILAMCE 2013)*, p. 1-14.

Rueda, J. A., Norena, N., Oliveira, M. F. F., & Roehl, D. M., 2014. Numerical models for detection of fault reactivation in oil and gas fields. In: *48th US Rock Mechanics Conference (ARMA 2014)*, p. 1-8.

Rueda, J. A., Oliveira, M. F. F, & Roehl, D. M., 2013. Geological fault reactivation with discrete and distributed numerical models. In: *XXXIV Iberian Latin American Congress on Computational Methods in Engineering* (*CILAMCE 2013)*, p. 1-14.

Rueda, J. A., 2013. *Reativação de falhas geológicas com modelos numéricos discretos e distribuído*. MSc. Thesis, Pontifical Catholic University of Rio de Janeir.

Segall, P.; Grasso, J-R.; & Mossop, A; 1994. Poroelastic stressing and induced seismicity near the Lacq gas fields, southwestern France. *Journal of Geophysical Research*, vol. 99, 423–438.

Sibson, R. H., 1977. Fault rocks and fault mechanisms. *Journal of the Geological Society of London*, vol. 133, pp. 191–213.

Wiprut, D., & Zoback, M. D., 2000. Fault reactivation and fluid flow along a previously dormant normal fault in the northern North Sea. *Geology*, vol. 28, 595–598.

Zhu, W., & Zhao, J., 2004. *Stability Analysis and Modelling of Underground Excavations in Fractured Rocks*. In Hudson, J. A. ed, Elsevier Geo-Engineering Book Series, vol. 1, Elsevier.